

Task-agnostic Unsupervised Out-of-Distribution Detection Using Kernel Density Estimation

Ertunc Erdil, Krishna Chaitanya, Neerav Karani, Ender Konukoglu

Computer Vision Lab, ETH Zurich

Sternwartstrasse 7, Zurich 8092, Switzerland

ertunc.erdil@vision.ee.ethz.ch

Abstract

In the recent years, researchers proposed a number of successful methods to perform out-of-distribution (OOD) detection in deep neural networks (DNNs). So far the scope of the highly accurate methods has been limited to classification tasks. Attempts for generally applicable methods beyond classification did not attain similar performance. In this paper, we propose a task-agnostic unsupervised OOD detection method using kernel density estimation (KDE) that addresses this limitation. We estimate the probability density functions (pdfs) of intermediate features of an already trained network, by performing KDE on the training dataset. As direct application of KDE to feature maps is hindered by their high dimensionality, we use a set of channel-wise marginalized KDE models instead of a single high-dimensional one. At test time, we evaluate the pdfs on a test sample and combine the resulting channel-wise scores with a logistic regression into a final confidence score that indicates the sample is OOD. Crucially, the proposed method is task agnostic as we only use intermediate features without requiring information on class labels nor the structure of the output, and attains high accuracy thanks to the flexibility of KDE. We performed experiments on DNNs trained for segmentation, detection and classification tasks, using benchmark datasets for OOD detection. The proposed method substantially outperformed existing works for non-classification networks while achieving on-par accuracy with the state-of-the-art for classification networks. The results demonstrate that the proposed method attains high OOD detection accuracy across different tasks, offering a larger scope of applications than existing task-specific methods and improving state-of-the-art for task-agnostic methods. The code will be made available.

1. Introduction

Deep neural networks (DNNs) can perform predictions on test images with very high accuracy when the training and testing data come from the same distribution. However, the prediction accuracy decreases rapidly if the test image is sampled from a different distribution. Furthermore, in such cases DNNs can make predictions with very high confidence [12]. This creates a big obstacle when deploying DNNs for real applications, especially for the ones with a low tolerance for error, such as autonomous driving and medical diagnosis. Therefore, it is crucial to improve the robustness of DNN-based methods and prevent them from making big mistakes [2]. Automatic detection of OOD samples can play a key role to this end. While substantial advances for classification-specific methods have been made recently, generic methods that can be used for any task still suffer from low detection accuracy. As a result, the scope of accurate OOD detection remains limited.

1.1. Related Work

We describe the OOD detection methods in the literature in three categories.

Methods that use predicted class probabilities: Hendrycks et al. [14] proposed a baseline OOD detection method that uses maximum predicted class probability in a classification DNN as a confidence score that the sample is OOD. ODIN [23] extends the baseline by applying an adversarial perturbation to the input image (referred to as input pre-processing) and temperature scaling at the output while computing OOD confidence scores. Both of these steps increase the difference between the scores of in-distribution (InD) and OOD samples. The work of Hsu et al. [17] further extends ODIN, referred to as Generalized ODIN (G-ODIN), by introducing an additional output that indicates whether the input sample belongs to InD or OOD. The penultimate layer of a DNN is decomposed into two branches to model the conditional distribution of this indicator variable and its joint distribution with the class

label. The conditional probability of the indicator variable is used as the confidence score while the ratio of the joint probability and the conditional probability serve as the final class prediction for an image after applying input processing.

Methods that propose training strategies: DeVries and Taylor [8] introduced a confidence estimation network branch, and proposed to use the confidence estimates obtained from this branch in order to train the softmax probabilities of the classification network. Lee et al. [21] presented a training method for classifier networks so that they become less confident for OOD examples. They introduced two loss terms in addition to the cross-entropy. The first one encourages the network to become less confident for the OOD examples whereas the second one generates the most optimal OOD examples for the first one. The method of Vyas et al. [30] uses an ensemble of classifiers for OOD detection, where each classifier is trained by leaving-out a different class from the InD training set. OOD detection is then performed based on the ensemble of softmax probabilities of each classifier, after applying temperature scaling and input pre-processing as in ODIN. Yu et al. [34] proposed a DNN with two classification heads, where one trains the network to minimize classification loss and to maximize the discrepancy between the two classifiers. The method, named as MCD, uses a subset of OOD samples along with the InD samples in the discrepancy loss. At test time, the samples with higher discrepancy are labeled as OOD.

Methods that perform density estimation: Lee et al. [22] proposed a method named as Mahalanobis, which models the class conditional pdfs of the features at intermediate layers of a DNN with Gaussian densities for InD samples. The parameters of each class conditional Gaussian are estimated by computing the empirical mean and co-variance using InD training samples belonging to that class. At test time, ODIN-style input pre-processing is applied before evaluating the estimated densities to obtain a confidence score, which is expected to be higher for InD samples and lower for OOD samples.

Despite their successful performance, all of the aforementioned methods are designed for OOD detection for classification tasks and they do not trivially extend to non-classification tasks. Task-agnostic networks that do not share the same drawback have also been proposed. Hendryks et al. [16] proposed a self-supervised learning (SSL) based OOD detection method. The method trains an auxiliary rotation network, which predicts angle of rotation in discrete categories, on the InD dataset and computes a confidence score for a test image as the maximum of the softmax activation, expecting higher activations for InD samples compared to OOD samples. Recently, Kim et al. [19] proposed a method, referred to as RaPP, that is based on the observation that in an auto-encoder the internal fea-

ture representations of an input image and its reconstructed version are very similar for InD samples and the similarity decreases for OOD samples that are not used for the training of the auto-encoder. RaPP defines a confidence score based on this observation for OOD detection. As both SSL and RaPP operate on auxiliary networks that are detached from the main network, they are task-agnostic and therefore can be applied to both classification and non-classification tasks. However, their detection accuracy, especially in non-classification tasks are limited as we empirically show.

1.2. Contribution

In this paper, we propose a novel task-agnostic unsupervised OOD detection method to address the above-mentioned limitations of existing methods. During training, we estimate feature pdfs for each channel of a given DNN using KDEs and training images, forming the InD dataset. For a new sample, each pdf yields a channel-wise confidence score and we combine all the scores in a final confidence score using a logistic regression model, which we train using training images as InD samples and their adversarially perturbed versions as pseudo-OOD samples. During testing, we compute the channel-wise confidence scores using the KDEs and pass them through the trained logistic regression model to decide whether a given sample is from InD or OOD. Training of the proposed OOD detection method is decoupled from the training of the DNN and only uses intermediate feature representations that the DNN extracts. Therefore, it can be applied to any network and without interfering with its training process. Also, while training the logistic regression, we do not require real OOD samples.

We take our motivation from Mahalanobis [22] for developing the proposed method but extend it in multiple ways crucial for building a task-agnostic method that achieves improved detection accuracy. 1) Mahalanobis estimates class conditional densities while the distribution approximation in the proposed method is not conditioned on the class, making it task-agnostic. 2) Direct use of Mahalanobis in the task-agnostic setting is feasible using unconditioned Gaussian distributions to approximate layer-wise feature distributions of InD samples. However, the Gaussian assumption may be too restrictive to model unconditioned feature densities and lead to lower accuracy when the assumption does not hold. Using KDEs, we extend the flexibility of the density approximation in the proposed method. 3) Layer-wise approximation is prone to the curse-of-dimensionality. Even though Mahalanobis takes channel-wise mean to reduce the dimension of a channel from $C \times H \times W$ to $C \times 1$ before density estimation, the resulting vector can still be high dimensional in modern architectures. We approximate 1D channel-wise distributions in the proposed method, which are simpler to estimate. This

approach ignores dependencies between channels of a layer in the density estimation part but takes them into account in the logistic regression model that combines channel-wise scores. Using KDE and estimating channel-wise pdfs are conceptually simple extensions that are very effective and yield substantial gains.

The use of KDEs for OOD detection is not new. The first use dates back to 1994 when Bishop [3] applied KDE in the input space. In that work, the input was only 12-dimensional and application of KDE was feasible. In modern architectures, the input dimensions are often much larger thereby, making the direct application of Bishop's method infeasible. The application of a modified version of the method in high dimensional spaces is still possible by applying KDE over the distances between the test image and the training images [18, 5]. Bishop's method as well as its modified version differs from the proposed method. Here we use multiple channel-wise KDEs and aggregate results, and this difference leads to substantially higher detection accuracy.

We performed extensive experiments on DNNs trained for 3 different tasks: segmentation, detection, and classification. We compare the performance of the proposed method with the state-of-the-art task-agnostic methods as well as the ones designed for classification tasks. In the experiments on segmentation and detection tasks, we use the COCO dataset [24] for training by using appropriate labelling according to the task, and 4 other datasets as OOD. We compare the proposed method with 4 different task-agnostic methods: RaPP [19], SSL [16], a modified version of Mahalanobis [22], and Bishop [3]. In the experiments on classification task, we use 2 different classification networks trained on CIFAR-10 and CIFAR-100 datasets [20] and 6 other OOD datasets. We compare with 5 OOD detection methods: Baseline [14], ODIN [23], Mahalanobis [22], MCD [34], and G-ODIN [17], which are all primarily designed for OOD detection in classification networks.

2. Method

Let us denote a set of training images with $X_{tr} = \{x_1, x_2, \dots, x_M\} \sim P_{in}$ and corresponding labels with $y_{tr} = \{y_1, y_2, \dots, y_M\}$, where P_{in} denotes the InD. Let us also denote a DNN with f , trained using (X_{tr}, y_{tr}) . f is more likely to perform good predictions on a test image x_{test} if $x_{test} \sim P_{in}$ and incorrect predictions if $x_{test} \sim P_{out}$, where $P_{out} \neq P_{in}$. In this section, we present the proposed task-agnostic KDE-based approach that identifies test images sampled from P_{out} . The application of the proposed model at test time is summarized in Algorithm 1.

2.1. Computing the confidence scores

The main output of the proposed method is a confidence score that indicates how likely a given sample belongs to

Algorithm 1: The proposed method

```

Input: Test Image:  $x$ 
Random subset of training images:
 $\hat{X}_{tr} = \{x_{u_1}, x_{u_2}, \dots, x_{u_N}\}$ 
Weights of logistic regression classifier:  $\alpha_{lc}$ 
Set of kernel sizes:  $\sigma$ 
Output: Confidence score of  $x$ :  $\mathcal{M}_x$ .
foreach  $l \in L$  do
  for  $c \leftarrow 1$  to  $C_l$  do
    Perform KDE at channel  $c$  of the feature
    map at layer  $l$ :
    
$$\hat{p}_{lc}(x) = \frac{1}{N} \sum_{i=1}^N \mathcal{K}(f_{lc}(x) - f_{lc}(x_{u_i}); \sigma_{lc})$$

  end
end
return  $\mathcal{M}_x = \sum_{l=1}^L \sum_{c=1}^{C_l} \alpha_{lc} \hat{p}_{lc}(x)$ 

```

OOD for the given DNN f . In this section, we describe how we compute this score. Let us assume that f consists of L layers and the feature map in a layer l for a given image x is denoted as $f_l(x)$ and it has dimensions $C_l \times H_l \times W_l$, where C_l , H_l , and W_l are the number of channels, height, and width of the feature map, respectively. We take the channel-wise mean of the feature map and reduce the dimensionality to $C_l \times 1$, as also done in [22]. We denote the resulting C_l -dimensional feature vector by $f'_l(x)$. We then estimate the marginal feature pdfs for each channel c using KDE:

$$p_{lc}(x) \approx \hat{p}_{lc}(x) = \frac{1}{M} \sum_{i=1}^M \mathcal{K}(f'_{lc}(x) - f'_{lc}(x_i); \sigma_{lc}) \quad (1)$$

where p_{lc} is the true marginal pdf of the features f'_{lc} in channel c of layer l , \hat{p}_{lc} is the estimate of the pdf, and $\mathcal{K}(u, v; \sigma_{lc}) = e^{-(u-v)^2/\sigma_{lc}^2}$ is a 1D squared exponential kernel with σ_{lc} being the kernel size. We describe the procedure to set the kernel size σ_{lc} in detail later in Section 2.3. When using KDE, we use samples $x_i \in X_{tr}$ and thus model InD channel-wise pdfs with \hat{p}_{lc} . For a given sample x , $\hat{p}_{lc}(x)$ is the confidence score of channel c in layer l .

The advantage of estimating channel-wise pdfs over estimating layer-wise pdfs, as was done in [22], is performing density estimation in 1D space instead of C_l -D space. Typically, C_l can be very large in modern networks, and density estimation becomes less accurate in high-dimensions [28], channel-wise estimation avoids this.

In order to evaluate p_{lc} in Eq. (1) for a new sample, ideally we need to store all the InD training images in X_{tr} . In real-world applications where M is very large, storing the entire X_{tr} may not be feasible and the summation over M images in Eq. (1) can take very long. Improving the computational and memory efficiency of KDE-based methods are possible by defining an unbiased estimator [9], which simply uses a

random subset of X_{tr} such that

$$\hat{X}_{tr} = \{x_{u_1}, x_{u_2}, \dots, x_{u_N}\} \subset X_{tr}$$

where $\{u_1, u_2, \dots, u_N\} \subset \{1, 2, \dots, M\}$ is a random subset of indices generated by sampling from a Uniform density, $\mathcal{U}(1, M)$, without replacement and $N \ll M$. Using the random subset, we replace the summation in Eq. (1) with the computationally more efficient unbiased estimator

$$p_{lc}(x) \approx \hat{p}_{lc}(x) = \frac{1}{N} \sum_{i=1}^N \mathcal{K}(f'_{lc}(x) - f'_{lc}(x_{u_i}); \sigma_{lc}). \quad (2)$$

In our experiments, we set $N = 5000$. In the supplementary material, we demonstrate that different choices of N do not change the OOD detection performance significantly.

Estimating marginal pdfs using Eq. (2) does not model dependencies between channels. In the proposed method, we take into account such dependencies and compute the final confidence score using a logistic regression classifier:

$$\mathcal{M}_x = \sum_{l=1}^L \sum_{c=1}^{C_l} \alpha_{lc} \hat{p}_{lc}(x) \quad (3)$$

where α_{lc} are the weights that are learned as described next.

2.2. Learning logistic regression weights α_{lc}

The role of the logistic regression model is to distinguish between InD and OOD samples given the channel-wise confidence scores. Training for the weights α_{lc} requires having access to both InD and OOD images. Although the InD images, X_{tr} , are already available, it is difficult to capture all possible images in P_{out} . Lee et al. [22] propose using adversarial examples obtained by FGSM [11] as samples from P_{out} to train the logistic regression classifier. We follow the same approach in the proposed method. After obtaining OOD samples by applying adversarial perturbation to the images in X_{tr} , the logistic regression classifier is trained by using the confidence scores \hat{p}_{lc} as inputs, and the output labels are provided as positive for InD images and negative for the OOD ones. We present further details on the FGSM method in the supplementary materials for completeness.

2.3. Determining size of KDE kernel σ_{lc}

Kernel size, σ , is a crucial parameter of KDE since it significantly affects the shape of the estimated density. Setting σ to a large value leads to very smooth pdfs, reducing the likelihood of the observed samples as well as other samples from the same distribution. Setting σ to a very small value leads to very peaky distributions only attributing high probability to observed samples, and assigning very low probability to unobserved samples even from the same distribution. Therefore, finding an optimal σ value is quite important in order to capture the underlying pdf of the data [28].

In the proposed method, as given in Eq. (2), we use a different σ_{lc} for each channel c and layer l . To compute σ_{lc} , we use the k -nearest neighbor method (kNN) [29]. Specifically, we compute the distance between $f'_{lc}(x_{u_i})$ and $f'_{lc}(x_{u_j})$ for all $i, j \in [1, N]$, $i \neq j$ and set σ_{lc} as the k^{th} smallest value. We denote the set of all σ_{lc} values by σ .

A parameter of the kNN method is the k itself. We automatically select the most appropriate k value from a set of candidate values denoted by \mathbf{k} . To achieve this, we split a validation set X_{val} from X_{tr} by taking the samples that are not used in KDE. Then, we apply adversarial perturbation to the images in X_{val} and obtain X_{val}^{adv} as OOD examples. We select the $k \in \mathbf{k}$ that maximizes the difference between the InD and OOD datasets.

$$k_{lc} = \arg \max_{k \in \mathbf{k}} \sum_{x \in X_{val}} \hat{p}_{lc}(x) - \sum_{x' \in X_{val}^{adv}} \hat{p}_{lc}(x') \quad (4)$$

where k_{lc} indicates the optimum k value in layer l . In our experiments, we choose k_l from the candidate set $\mathbf{k} = \{1, 2, 5, 10, 15, 20, 50\}$ using the described method.

3. Experimental results

3.1. Datasets and network architectures

We evaluate the performance of the proposed approach on DNNs trained for three different tasks: segmentation, detection, and classification. The proposed method is implemented in PyTorch and we run all experiments on a Nvidia GeForce Titan X GPU with 12GB memory.

Segmentation and detection experiments: In the segmentation experiments, we use the DeeplabV3 [4] architecture that has ResNet [13] backbone while in the detection experiments, we use Faster R-CNN [27]. Both DeeplabV3 and Faster R-CNN models are pre-trained on the COCO dataset [24] by using appropriate labelling according to the task. COCO dataset contains 118287 annotated training images and 40670 test images and the pre-trained models are available in PyTorch.

We compare the proposed method with 4 different OOD detection methods: RaPP [19], SSL [16], a modified version of Mahalanobis [22], and Bishop [3]. In the experiments with RaPP, we train an auto-encoder network on the InD dataset (COCO) by using a 10-layer encoder-decoder network architecture as in the original paper [19]. SSL uses a self-supervised rotation network for OOD detection. To compare with SSL, we randomly rotate the training images in the InD dataset and train a neural network that predicts the rotation angle using a ResNet architecture. As we discussed in Section 1.1, both SSL and RaPP are task-agnostic methods that perform detection using auxiliary networks. In our experiments, we use the architectures suggested in the original papers for the auxiliary networks. Mahalanobis

is originally proposed for OOD detection in classification networks, requiring class labels for each sample in the InD dataset. To modify Mahalanobis for non-classification tasks, we assign the same class to all images. Lastly, we also compare our method with Bishop’s work [3] to demonstrate the value of applying KDE on the intermediate features using the proposed method rather than the input.

We use 4 datasets as OOD. Pascal VOC [10] dataset contains 1449 test images. KITTI [1] contains 200 test images of street scenes. Berkeley Deep Drive (BDD) [32] is another dataset that contains images of street scenes and includes 2000 test images. Finally, Places [35] datasets that we use as OOD contains 328500 test images. We use a random subset of 10000 images of the Places dataset in our experiments for computational purposes.

Classification experiments: In the classification experiments, we use two different ResNet architectures trained on CIFAR-100 and CIFAR-10 [20] datasets that contain images from 100 and 10 classes, respectively. Both datasets contain 50000 training and 10000 test images where each one is a 32×32 color image¹.

We compare the proposed method with the Baseline method proposed by Hendryks et al. [14], ODIN [23], Mahalanobis [22], MCD [34], and G-ODIN [17] which are primarily designed for OOD detection in classification networks. ODIN and Mahalanobis have user defined parameters that affect their performance. These parameters are temperature scaling and input pre-processing magnitude for ODIN, and only the input pre-processing magnitude for Mahalanobis. We choose these parameters from the list of values given in the original papers by using a validation set that contains samples from InD and adversarial images. The best-performing parameters in terms of FPR at 95% TPR are chosen for each InD dataset. The implementation of G-ODIN is not publicly available but as our experimental settings are very similar to theirs [17], including network architectures and OOD datasets, we directly use the results presented in their paper for comparison. MCD requires samples from the target OOD dataset during training, however, such samples may not be available in a real application. For a fair comparison, we use the same pseudo OOD samples used to train the logistic regression model in our method to also train the MCD. As explained in Sec. 2.2, the pseudo OOD samples were generated by adversarially perturbing the InD images. We use 6 different datasets as OOD²: SVHN [26] contains 26032 images of house numbers in Google street-view images. Resized TinyImageNet (Tin-rs) and cropped TinyImageNet (Tin-cr) consist of 10000 32×32 RGB test images which are obtained by resizing and cropping a sub-

¹Pretrained models are available at https://github.com/pokaxpoka/deep_Mahalanobis_detector

²Tin-rs, Tin-cr, LSUN-rs, LSUN-cr, and iSUN are available at <https://github.com/facebookresearch/odin>

set of the original ImageNet dataset [7], respectively. Resized LSUN (LSUN-rs) and cropped LSUN (LSN-cr) contain 10000 RGB test images with size 32×32 and they are obtained by resizing and cropping a subset of the original LSUN dataset [33]. iSUN is a subset of SUN dataset [31] that contains 8925 RGB images resized to 32×32 .

3.2. Evaluation methods

We use the evaluation methods that are commonly used for evaluating OOD detection methods in the literature [14]. In all evaluations, we take the InD as the positive class and OOD as the negative class.

FPR at 95% TPR: False positive rate (FPR) is measured when the true positive rate (TPR) of 95% is reached at a certain threshold. The false positive rate is calculated as $FPR = FP / (FP + TN)$ and true positive rate is calculated as $TPR = TP / (TP + FN)$ where TP, FP, TN, and FN represent true positive, false positive, true negative, and false negative, respectively.

Detection error: This metric measures the probability of wrong classification when TPR is 95%. We denote the detection error by P_{err} and compute as $P_{err} = 0.5(1 - TPR + FPR)$.

AUROC: The Area Under the Receiver Operating Characteristic curve (AUROC) is a threshold independent method that measures the area below Receiver Operating Characteristic (ROC) curve [6]. ROC curve reflects the relationship between TPR and FPR values as the threshold changes. AUROC takes its highest value at 100% when the detection is perfect.

3.3. Results and Analysis

Here we present the main quantitative results for all three tasks and present additional experimental results in the supplementary materials.

3.3.1 Results on segmentation and detection tasks

The quantitative results of the segmentation experiments on the DeepLabV3 architecture are shown in Table 1. The results demonstrate that the proposed method achieves significant improvement over the existing methods from Bishop, RaPP, SSL, and Mahalanobis. The first task-agnostic method, RaPP, operates on an auto-encoder network and perform OOD detection by computing the distances between input image and its reconstruction at different layers. However, the distances may not be discriminative to distinguish OOD samples as shown by the quantitative results in Table 1. The second task-agnostic method, SSL, uses output probabilities of a self-supervised auxiliary rotation network for OOD detection. DNNs may not learn dataset-specific features to perform well on a rotation task and can generalize to other OOD datasets. This is the case

OOD	FPR at 95% TPR \downarrow	AUROC \uparrow		Detection Error \downarrow
		Bishop [3] / SSL / Mahalanobis / RaPP / Proposed		
Pascal	97.17 / 95.42 / 96.05 / 95.30 / 13.92	46.61 / 50.87 / 52.99 / 56.94 / 97.27	51.08 / 50.21 / 50.52 / 50.15 / 9.48	
KITTI	95.00 / 88.81 / 97.91 / 53.15 / 42.65	74.08 / 58.29 / 21.55 / 84.28 / 94.35	50.00 / 46.90 / 51.35 / 29.07 / 23.82	
BDD	99.20 / 94.07 / 89.53 / 89.41 / 38.58	47.55 / 51.95 / 51.50 / 49.79 / 95.71	52.10 / 49.53 / 47.26 / 47.20 / 21.79	
Places	96.37 / 94.67 / 96.23 / 93.22 / 12.46	48.86 / 50.68 / 47.81 / 62.23 / 97.55	50.68 / 49.83 / 50.61 / 49.11 / 8.73	

Table 1: Quantitative results on distinguishing test set of COCO InD dataset from several OOD datasets **in the DeepLabV3 segmentation network**. \uparrow indicates larger value is better and \downarrow indicates lower value is better. *All values are percentages.*

OOD	FPR at 95% TPR \downarrow	AUROC \uparrow	
		Mahalanobis	Proposed
Pascal	94.29 / 5.24	48.49 / 99.00	
KITTI	98.74 / 4.61	14.58 / 99.06	
BDD	91.27 / 8.78	46.52 / 98.35	
Places	96.23 / 1.84	46.35 / 99.07	

Table 2: Quantitative results on distinguishing test set of COCO InD dataset from several OOD datasets **in the Faster R-CNN detection network**. We do not include the results of RaPP and SSL in this table since their performance on the same dataset does not change for different architectures nor tasks. They produce the same results on COCO for both segmentation and detection tasks which are already given in Table 1.

with the rotation network in SSL because the accuracy of the rotation network is $\sim 75\%$ for both the InD test set and the OOD datasets, which makes it hard to distinguish OOD images by looking at the softmax outputs. In Mahalanobis, we assign the same label to all images in InD dataset and estimate the feature densities at different layers using a single Gaussian per layer since the class label information is not available in the segmentation task. The lower OOD detection accuracy with this method suggests that the Gaussian assumption may not be optimal to model the feature densities. The proposed method achieves quite a substantial improvement over the other methods, suggesting estimating channel-wise feature densities with KDE is better suited than using a single Gaussian per layer, using KDE on the input space as well as using auxiliary networks.

We present the quantitative results of the detection experiments on the Faster R-CNN architecture in Table 2. Recall that RaPP and SSL methods operate on auxiliary DNNs that are detached from the main network. Since we are using the same InD and OOD datasets in our experiments with segmentation and detection tasks, the auxiliary networks are the same and therefore detection performance of these methods are also the same in both experiments, despite the change in the task. This also applies to Bishop since it performs KDE in the input space. This means that the results of the RaPP, SSL, and Bishop for the detection

task are same as the results for the segmentation task shown in Table 1. Therefore, we do not re-write these results in Table 2 for conciseness. Similar to the segmentation network experiments, the proposed method performs substantially better than RaPP, SSL, and Mahalanobis on the detection networks. We perform additional experiments on another detection network architecture, Mask R-CNN, and present the results in the supplementary material.

The quantitative results in both segmentation and detection tasks demonstrate that the proposed task-agnostic KDE-based OOD detection method advances the existing task-agnostic methods by a large margin.

3.3.2 Results on classification tasks

We perform experiments on classification tasks by using two different InD datasets: CIFAR-100 and CIFAR-10. We present the quantitative OOD detections results of Baseline, ODIN, Mahalanobis, MCD, G-ODIN, and the proposed method for CIFAR-100 experiment in Table 3. The results demonstrate that the proposed methods achieves better OOD detection performance on 4 out of 6 OOD datasets (SVHN, TIN-rs, LSUN-rs, and iSUN). Performance of the proposed method diminishes on TIN-cr and LSUN-cr datasets, where ODIN achieves the best performance.

In Table 4, we present the results of CIFAR-10 experiments. Here, our task-agnostic KDE-based method produces the best OOD detection results on TIN-rs, LSUN-rs, and iSUN datasets, and the second best results on SVHN dataset. Similar to the CIFAR-100 experiments, ODIN achieves the best results on TIN-cr and LSUN-cr datasets whereas the proposed method suffers from low accuracy. We present additional results of both CIFAR-100 and CIFAR-10 experiments with respect to *Detection Error* metric in the supplementary material. The results on the classification tasks suggest that the method’s performance is on par with state-of-the-art OOD detection methods despite not being classification-specific as the others.

The logistic regression model in the proposed method is trained with the InD images and their adversarially perturbed versions as OOD samples. Even though the OOD space is vast, training with the perturbed samples seems to perform well. To better understand how the regression

OOD	FPR at 95% TPR \downarrow					AUROC \uparrow						
	Baseline / ODIN / Mahalanobis / MCD / G-ODIN / Proposed											
SVHN	55.73	/ 24.76	/ 9.00	/ 75.00	/ 44.90	/ 4.87	79.34	/ 92.13	/ 97.63	/ 63.47	/ 93.20	/ 98.05
TIN-rs	58.97	/ 26.85	/ 24.90	/ 49.68	/ 23.50	/ 6.18	77.07	/ 88.32	/ 94.63	/ 87.57	/ 95.9	/ 98.18
TIN-cr	52.69	/ 26.85	/ 44.24	/ 40.82	/ 27.40	/ 78.15	82.02	/ 92.00	/ 91.15	/ 86.91	/ 95.30	/ 75.01
LSUN-rs	64.71	/ 37.09	/ 26.66	/ 44.87	/ 23.20	/ 1.70	75.58	/ 87.77	/ 93.08	/ 88.94	/ 96.10	/ 99.41
LSUN-cr	66.95	/ 34.78	/ 32.58	/ 50.05	/ 34.30	/ 65.22	77.19	/ 88.94	/ 92.19	/ 79.55	/ 93.80	/ 81.54
iSUN	63.26	/ 38.21	/ 28.86	/ 59.60	/ 24.70	/ 4.41	75.68	/ 86.73	/ 93.31	/ 84.68	/ 95.70	/ 98.91

Table 3: Quantitative results on distinguishing test set of CIFAR-100 InD dataset from several OOD datasets. \uparrow indicates larger value is better and \downarrow indicates lower value is better. *All values are percentages.*

OOD	FPR at 95% TPR \downarrow					AUROC \uparrow						
	Baseline / ODIN / Mahalanobis / MCD / G-ODIN / Proposed											
SVHN	25.77	/ 17.65	/ 4.09	/ 75.78	/ 10.50	/ 6.80	89.88	/ 95.42	/ 99.04	/ 71.15	/ 97.80	/ 97.87
TIN-rs	28.37	/ 11.24	/ 59.55	/ 32.30	/ 18.60	/ 1.91	90.95	/ 96.78	/ 81.21	/ 92.46	/ 96.10	/ 99.05
TIN-cr	24.29	/ 7.56	/ 33.29	/ 22.61	/ 18.90	/ 72.01	92.33	/ 98.07	/ 88.82	/ 90.30	/ 96.00	/ 78.88
LSUN-rs	28.31	/ 10.39	/ 29.68	/ 22.93	/ 9.10	/ 1.12	91.05	/ 97.06	/ 92.94	/ 94.99	/ 96.0	/ 99.62
LSUN-cr	16.75	/ 4.67	/ 14.78	/ 25.15	/ 12.7	/ 79.79	94.35	/ 98.71	/ 96.38	/ 88.56	/ 97.2	/ 71.63
iSUN	28.02	/ 12.37	/ 30.81	/ 25.75	/ 11.2	/ 2.06	91.01	/ 96.03	/ 92.64	/ 94.52	/ 97.6	/ 98.93

Table 4: Quantitative results on distinguishing test set of CIFAR-10 InD dataset from several OOD datasets. \uparrow indicates larger value is better and \downarrow indicates lower value is better. *All values are percentages.*

model generalizes to real OOD images, we analyzed the channel-wise confidence scores $\hat{p}_{lc}(x)$, which are the inputs to the regression model. We performed OOD detection with each channel’s confidence score separately and plot the AUROC values for SVHN, TIN-rs, TIN-cr, LSUN-rs, LSUN-cr, iSUN datasets, and the adversarial images when the InD is CIFAR-10 in Fig. 1. It can be seen that the AUROC trends across channels for SVHN, TIN-rs, LSUN-rs, and iSUN are similar to the adversarial images, where AUROC results are lower in the earlier channels and higher in the later ones. The similarity between the trends explains the high OOD detection performance of the proposed method in these datasets. On the contrary, AUROC results are higher in the earlier channels for the TIN-cr and LSUN-cr datasets and the trends are not aligned with the adversarial images. The difference between the trends negatively affects the generalization performance of the logistic regression classifier to these datasets and results in diminished OOD detection performance. The reason of having higher AUROC scores in the earlier layers for TIN-cr and LSUN-cr datasets could be that these cropped images do not contain many low-level features such as edges and corners unlike the InD images - instead, they mostly consist of smooth regions. Since the earlier layers of the networks extract such features, higher OOD detection performances are obtained in the earlier channels for these datasets. We present a similar analysis of the results on CIFAR-100 dataset in the supplementary material.

	Layer-wise		Channel-wise	
	Gaussian (Mahalanobis)	KDE	Gaussian	KDE (Proposed)
SVHN	9.00	24.09	6.09	4.87
TIN-rs	24.90	34.08	10.60	6.18
LSUN-rs	26.66	28.47	1.45	1.70
iSUN	28.86	33.49	4.99	4.41

Table 5: Comparison between different combinations of density estimation methods (Gaussian and KDE) with feature spaces (layer-wise and channel-wise) in terms of FPR at 95% TPR in CIFAR-100 dataset.

3.4. Channel-wise vs layer-wise and KDE vs parametric estimation

In the proposed method, we perform channel-wise KDE. Compared to the closest work Mahalanobis [22], this introduces two changes in the density estimation, one in feature selection (layer-wise vs channel features) and the other in estimation methodology (KDE vs Gaussian). In this section, we quantify the contribution of each change. To this end, we perform OOD detection with all possible combinations. The results in Table 5 demonstrate that performing channel-wise density estimation leads to a large improvement on OOD detection accuracy compared to layer-wise density estimation. We argue that this improvement is due to achieving more accurate density estimation in 1D

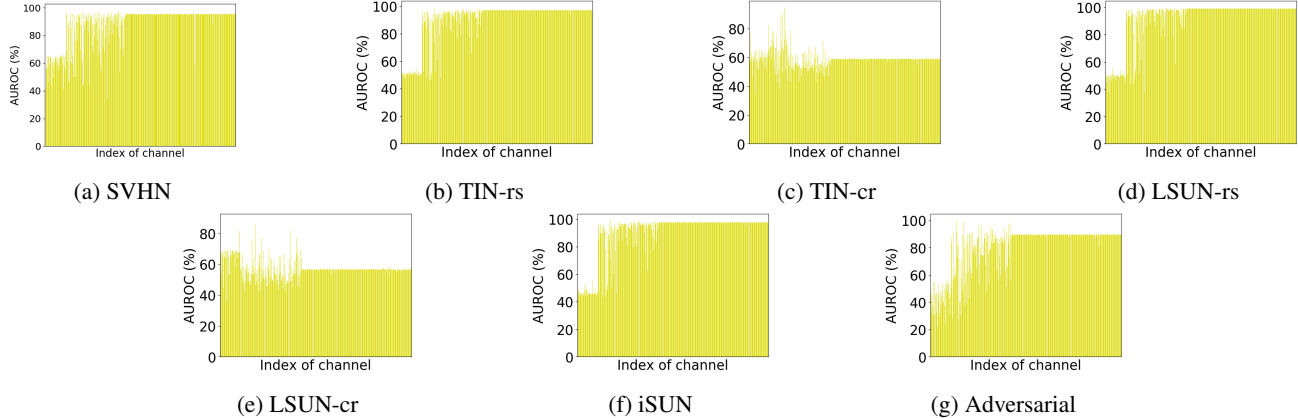


Figure 1: Trends of channel-wise OOD detection performance evaluated with AUROC for different OOD datasets when the InD dataset is CIFAR-10. The plots show that the AUROC trend of adversarial images is similar to most of the OOD datasets, indicating that the logistic regression classifier trained using adversarial images can generalize to most of the OOD datasets.

space with the channel-wise features. Dependencies between channels are taken into account in the logistic regression model. We also observe that performing KDE on the channel-wise features yields further improvements over using Gaussian for most cases. This is expected since KDE is more flexible and can lead to more accurate density estimations. We present further experiments to compare channel-wise vs layer-wise KDE in the supplementary material.

3.5. Computation time

We compare the proposed method with the others in terms of computation time. We measure the computation time needed to perform detection on all OOD datasets in the CIFAR-10 experiments for Baseline, ODIN, MCD, and Mahalanobis. We cannot obtain the computation time of G-ODIN since the implementation is not publicly available. We show the mean and standard deviation of the computation times in the plot in Fig. 2. The results demonstrate that the Baseline and MCD are the fastest methods as expected since they do only a single forward pass in the networks. The proposed method is the third most efficient method despite the computational cost of KDE. The main reason for ODIN and Mahalanobis being computationally less efficient than the proposed method is the input pre-processing step, which can be computationally costly. Mahalanobis is the slowest method among all since it applies input pre-processing before computing the scores at each layer.

4. Conclusion

In this paper, we presented a task-agnostic unsupervised OOD detection method that estimates feature densities for each channel of a DNN using KDE. Features of a test image are evaluated at the corresponding KDEs to obtain a confidence score per channel, which is expected to be higher for

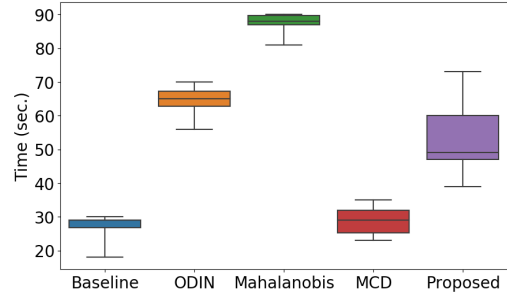


Figure 2: Mean and standard deviation of the computation times of all OOD datasets in the CIFAR-10 experiments.

InD images than OOD ones. These scores are combined into a final score using logistic regression classifier, that is pre-trained using InD training images and their adversarially perturbed versions. Being task-agnostic, the proposed method can be applied to both classification and non-classification DNNs.

We perform an extensive evaluation on both classification and non-classification (segmentation and detection) networks and compare them with the state-of-the-art methods. In the segmentation and detection tasks, our method achieves substantial improvement over the existing task-agnostic methods. In the classification tasks, the proposed method achieves OOD detection results on-par with the state-of-the-art. The results demonstrate that the proposed method attains high OOD detection accuracy across different tasks, exhibiting a larger scope of applications than existing task-specific methods and improving state-of-the-art for task-agnostic methods.

References

[1] Hassan Abu Alhaija, Siva Karthik Mustikovela, Lars Mescheder, Andreas Geiger, and Carsten Rother. Augmented reality meets computer vision: Efficient data generation for urban driving scenes. *International Journal of Computer Vision*, 126(9):961–972, 2018. 5

[2] Dario Amodei, Chris Olah, Jacob Steinhardt, Paul Christiano, John Schulman, and Dan Mané. Concrete problems in ai safety. *arXiv preprint arXiv:1606.06565*, 2016. 1

[3] Christopher M Bishop. Novelty detection and neural network validation. *IEE Proceedings-Vision, Image and Signal processing*, 141(4):217–222, 1994. 3, 4, 5, 6

[4] Liang-Chieh Chen, George Papandreou, Florian Schroff, and Hartwig Adam. Rethinking atrous convolution for semantic image segmentation. *arXiv preprint arXiv:1706.05587*, 2017. 4

[5] Daniel Cremers, Stanley J Osher, and Stefano Soatto. Kernel density estimation and intrinsic alignment for shape priors in level set segmentation. *International journal of computer vision*, 69(3):335–351, 2006. 3

[6] Jesse Davis and Mark Goadrich. The relationship between precision-recall and roc curves. In *Proceedings of the 23rd international conference on Machine learning*, pages 233–240. ACM, 2006. 5

[7] Jia Deng, Wei Dong, Richard Socher, Li-Jia Li, Kai Li, and Li Fei-Fei. Imagenet: A large-scale hierarchical image database. In *2009 IEEE conference on computer vision and pattern recognition*, pages 248–255. Ieee, 2009. 5

[8] Terrance DeVries and Graham W Taylor. Learning confidence for out-of-distribution detection in neural networks. *arXiv preprint arXiv:1802.04865*, 2018. 2

[9] Ertunc Erdil, Sinan Yildirim, Tolga Tasdizen, and Mujdat Cetin. Pseudo-marginal mcmc sampling for image segmentation using nonparametric shape priors. *IEEE Transactions on Image Processing*, 28(11):5702–5715, 2019. 3

[10] Mark Everingham, Luc Van Gool, Christopher KI Williams, John Winn, and Andrew Zisserman. The pascal visual object classes (voc) challenge. *International journal of computer vision*, 88(2):303–338, 2010. 5

[11] Ian J Goodfellow, Jonathon Shlens, and Christian Szegedy. Explaining and harnessing adversarial examples. *arXiv preprint arXiv:1412.6572*, 2014. 4, 13

[12] Chuan Guo, Geoff Pleiss, Yu Sun, and Kilian Q Weinberger. On calibration of modern neural networks. In *Proceedings of the 34th International Conference on Machine Learning-Volume 70*, pages 1321–1330. JMLR. org, 2017. 1

[13] Kaiming He, Xiangyu Zhang, Shaoqing Ren, and Jian Sun. Deep residual learning for image recognition. In *Proceedings of the IEEE conference on computer vision and pattern recognition*, pages 770–778, 2016. 4

[14] Dan Hendrycks and Kevin Gimpel. A baseline for detecting misclassified and out-of-distribution examples in neural networks. *Proceedings of International Conference on Learning Representations*, 2017. 1, 3, 5

[15] Dan Hendrycks, Mantas Mazeika, and Thomas Dietterich. Deep anomaly detection with outlier exposure. *arXiv preprint arXiv:1812.04606*, 2018. 13, 14

[16] Dan Hendrycks, Mantas Mazeika, Saurav Kadavath, and Dawn Song. Using self-supervised learning can improve model robustness and uncertainty. In *Advances in Neural Information Processing Systems*, pages 15637–15648, 2019. 2, 3, 4

[17] Yen-Chang Hsu, Yilin Shen, Hongxia Jin, and Zsolt Kira. Generalized odin: Detecting out-of-distribution image without learning from out-of-distribution data. In *Proceedings of the IEEE/CVF Conference on Computer Vision and Pattern Recognition*, pages 10951–10960, 2020. 1, 3, 5

[18] Junmo Kim, Müjdat Çetin, and Alan S Willsky. Nonparametric shape priors for active contour-based image segmentation. *Signal Processing*, 87(12):3021–3044, 2007. 3

[19] Ki Hyun Kim, Sangwoo Shim, Yongsuk Lim, Jongseob Jeon, Jeongwoo Choi, Byungchan Kim, and Andre S Yoon. Rapp: Novelty detection with reconstruction along projection pathway. In *International Conference on Learning Representations*, 2020. 2, 3, 4

[20] Alex Krizhevsky, Geoffrey Hinton, et al. Learning multiple layers of features from tiny images. Technical report, Citeseer, 2009. 3, 5

[21] Kimin Lee, Honglak Lee, Kibok Lee, and Jinwoo Shin. Training confidence-calibrated classifiers for detecting out-of-distribution samples. In *ICLR 2018*. ICLR 2018, 2018. 2

[22] Kimin Lee, Kibok Lee, Honglak Lee, and Jinwoo Shin. A simple unified framework for detecting out-of-distribution samples and adversarial attacks. In *Advances in Neural Information Processing Systems*, pages 7167–7177, 2018. 2, 3, 4, 5, 7

[23] Shiyu Liang, Yixuan Li, and Rayadurgam Srikant. Enhancing the reliability of out-of-distribution image detection in neural networks. *arXiv preprint arXiv:1706.02690*, 2017. 1, 3, 5

[24] Tsung-Yi Lin, Michael Maire, Serge Belongie, James Hays, Pietro Perona, Deva Ramanan, Piotr Dollár, and C Lawrence Zitnick. Microsoft coco: Common objects in context. In *European conference on computer vision*, pages 740–755. Springer, 2014. 3, 4

[25] Eric Nalisnick, Akihiro Matsukawa, Yee Whye Teh, Dilan Gorur, and Balaji Lakshminarayanan. Do deep generative models know what they don’t know? *arXiv preprint arXiv:1810.09136*, 2018. 13

[26] Yuval Netzer, Tao Wang, Adam Coates, Alessandro Bissacco, Bo Wu, and Andrew Y Ng. Reading digits in natural images with unsupervised feature learning. 2011. 5

[27] Shaoqing Ren, Kaiming He, Ross Girshick, and Jian Sun. Faster r-cnn: Towards real-time object detection with region proposal networks. In *Advances in neural information processing systems*, pages 91–99, 2015. 4

[28] David W Scott. *Multivariate density estimation: theory, practice, and visualization*. John Wiley & Sons, 2015. 3, 4

[29] Bernard W Silverman. *Density estimation for statistics and data analysis*, volume 26. CRC press, 1986. 4

[30] Apoorv Vyas, Nataraj Jammalamadaka, Xia Zhu, Dipankar Das, Bharat Kaul, and Theodore L Willke. Out-of-distribution detection using an ensemble of self supervised

leave-out classifiers. In *Proceedings of the European Conference on Computer Vision (ECCV)*, pages 550–564, 2018.

2

- [31] Pingmei Xu, Krista A Ehinger, Yinda Zhang, Adam Finkelstein, Sanjeev R Kulkarni, and Jianxiong Xiao. Turkergaze: Crowdsourcing saliency with webcam based eye tracking. *arXiv preprint arXiv:1504.06755*, 2015. 5
- [32] Fisher Yu, Haofeng Chen, Xin Wang, Wenqi Xian, Yingying Chen, Fangchen Liu, Vashisht Madhavan, and Trevor Darrell. Bdd100k: A diverse driving dataset for heterogeneous multitask learning. In *The IEEE Conference on Computer Vision and Pattern Recognition (CVPR)*, 2020. 5
- [33] Fisher Yu, Ari Seff, Yinda Zhang, Shuran Song, Thomas Funkhouser, and Jianxiong Xiao. Lsun: Construction of a large-scale image dataset using deep learning with humans in the loop. *arXiv preprint arXiv:1506.03365*, 2015. 5
- [34] Qing Yu and Kiyoharu Aizawa. Unsupervised out-of-distribution detection by maximum classifier discrepancy. In *Proceedings of the IEEE International Conference on Computer Vision*, pages 9518–9526, 2019. 2, 3, 5
- [35] Bolei Zhou, Agata Lapedriza, Aditya Khosla, Aude Oliva, and Antonio Torralba. Places: A 10 million image database for scene recognition. *IEEE transactions on pattern analysis and machine intelligence*, 40(6):1452–1464, 2017. 5

A. Experiments on Mask R-CNN trained on COCO

In this section, we present experiments on a new detection network architecture, Mask R-CNN, trained on COCO datasets. We compare our results with SSL and Mahalanobis as shown in Table 6. In this network architecture, the proposed method achieves OOD detection almost without any error while the other methods do not perform well.

OOD	FPR at 95% TPR \downarrow	AUROC \uparrow					Detection Error \downarrow
		Bishop / SSL / Mahalanobis / RaPP / Proposed					
Pascal	97.17 / 95.42 / 94.23 / 95.30 / 0.0	46.61 / 50.87 / 49.06 / 56.94 / 99.70	51.08 / 50.21 / 49.61 / 50.15 / 2.50				
KITTI	95.00 / 88.81 / 99.29 / 53.15 / 0.0	74.08 / 58.29 / 14.75 / 84.28 / 99.01	50.00 / 46.90 / 52.14 / 29.07 / 2.50				
BDD	99.20 / 94.07 / 94.69 / 89.41 / 0.0	47.55 / 51.95 / 44.40 / 49.79 / 99.64	52.10 / 49.53 / 49.84 / 47.20 / 2.50				
Places	96.37 / 94.67 / 95.04 / 93.22 / 0.0	48.86 / 50.68 / 47.69 / 62.23 / 99.75	50.68 / 49.83 / 50.02 / 49.11 / 2.50				

Table 6: Quantitative results on distinguishing test set of COCO InD dataset from several OOD datasets in the detection network trained on **Mask R-CNN** architecture.

B. Detection error results of the CIFAR-100 and CIFAR-10 experiments

In this section, we present additional results using detection error metric for CIFAR-100 and CIFAR-10 experiments presented in Sec. 3.3.2. of the main paper. The additional results are presented in Tables 7 and 8, respectively. The results are aligned with the results presented in the paper using the other metrics.

OOD	Detection Error \downarrow					
	Baseline / ODIN / Mahalanobis / MCD / G-ODIN / Proposed					
SVHN	30.36 / 14.88 / 7.00 / 40.00 / - / 4.93					
TIN-rs	31.98 / 19.37 / 14.95 / 27.34 / - / 5.58					
TIN-cr	28.84 / 15.92 / 16.04 / 22.91 / - / 41.57					
LSUN-rs	34.85 / 21.04 / 15.83 / 24.93 / - / 3.35					
LSUN-cr	35.97 / 19.89 / 10.95 / 27.52 / - / 35.11					
iSUN	34.13 / 21.06 / 16.93 / 32.30 / - / 4.70					

Table 7: Additional quantitative results of the CIFAR-100 experiments presented in the main paper with respect to Detection Error. Note that the results of G-ODIN are not included since the original paper does not report Detection Error results.

OOD	Detection Error \downarrow					
	Baseline / ODIN / Mahalanobis / MCD / G-ODIN / Proposed					
SVHN	15.38 / 11.32 / 4.54 / 40.39 / - / 5.90					
TIN-rs	16.68 / 8.12 / 32.27 / 18.65 / - / 3.45					
TIN-cr	16.64 / 6.28 / 19.14 / 13.80 / - / 38.50					
LSUN-rs	16.65 / 7.69 / 17.34 / 13.96 / - / 3.06					
LSUN-cr	10.87 / 4.83 / 9.89 / 15.07 / - / 42.39					
iSUN	16.51 / 8.68 / 17.90 / 15.37 / - / 3.53					

Table 8: Additional quantitative results of the CIFAR-10 experiments presented in the main paper with respect to Detection Error. Note that the results of G-ODIN are not included since the original paper does not report Detection Error results.

C. Analysis with different N

N is a hyperparameter of the proposed method that determines number of samples to be used for unbiased estimation of the target density using KDE. In this section, we analyze the behavior of the proposed approach as a function of different N values. We present the OOD detection performance using different metrics for both CIFAR-10 and CIFAR-100 experiments in Tables 9 and 10, respectively.

OOD	FPR at 95% TPR ↓	AUROC ↑				Detection Error ↓
		$N = 1000/2000/5000/7000$				
SVHN	24.58 / 14.90 / 6.80 / 7.00	92.84 / 95.91 / 97.87 / 97.99				14.79 / 9.95 / 5.90 / 6.00
TIN-rs	1.39 / 1.31 / 1.91 / 2.33	99.15 / 99.28 / 99.05 / 99.20				3.19 / 3.15 / 3.45 / 3.66
TIN-cr	75.03 / 76.60 / 72.01 / 71.41	78.47 / 78.07 / 78.88 / 79.40				40.01 / 40.80 / 38.50 / 38.20
LSUN-rs	0.49 / 0.56 / 1.12 / 1.41	99.72 / 99.73 / 99.62 / 99.60				2.74 / 2.78 / 3.06 / 3.20
LSUN-cr	80.63 / 78.35 / 79.79 / 80.67	69.83 / 71.94 / 71.63 / 70.30				42.81 / 41.67 / 42.39 / 42.83
iSUN	1.38 / 1.26 / 2.06 / 2.48	99.17 / 99.24 / 98.93 / 99.05				3.19 / 3.13 / 3.53 / 3.74

Table 9: Performance of the proposed method on CIFAR-10 dataset as a function of number of samples (N) that are used in KDE.

OOD	FPR at 95% TPR ↓	AUROC ↑				Detection Error ↓
		$N = 1000/2000/5000/7000$				
SVHN	8.61 / 8.71 / 4.87 / 4.67	95.75 / 97.15 / 98.05 / 98.49				6.80 / 6.85 / 4.93 / 4.83
TIN-rs	6.31 / 4.87 / 6.16 / 9.11	98.16 / 98.63 / 98.18 / 98.12				5.65 / 4.93 / 5.58 / 7.05
TIN-cr	80.44 / 78.52 / 78.15 / 75.87	74.68 / 72.68 / 75.01 / 75.70				42.72 / 41.76 / 41.57 / 40.43
LSUN-rs	4.03 / 1.20 / 1.70 / 2.51	98.69 / 99.51 / 99.41 / 99.27				4.51 / 3.10 / 3.35 / 3.75
LSUN-cr	76.11 / 66.82 / 65.22 / 61.62	71.96 / 80.33 / 81.54 / 82.68				40.55 / 35.91 / 35.11 / 33.31
iSUN	5.32 / 4.28 / 4.41 / 7.68	98.45 / 99.15 / 98.91 / 98.65				5.16 / 4.64 / 4.70 / 6.34

Table 10: Performance of the proposed method on CIFAR-100 dataset as a function of number of samples (N) that are used in KDE.

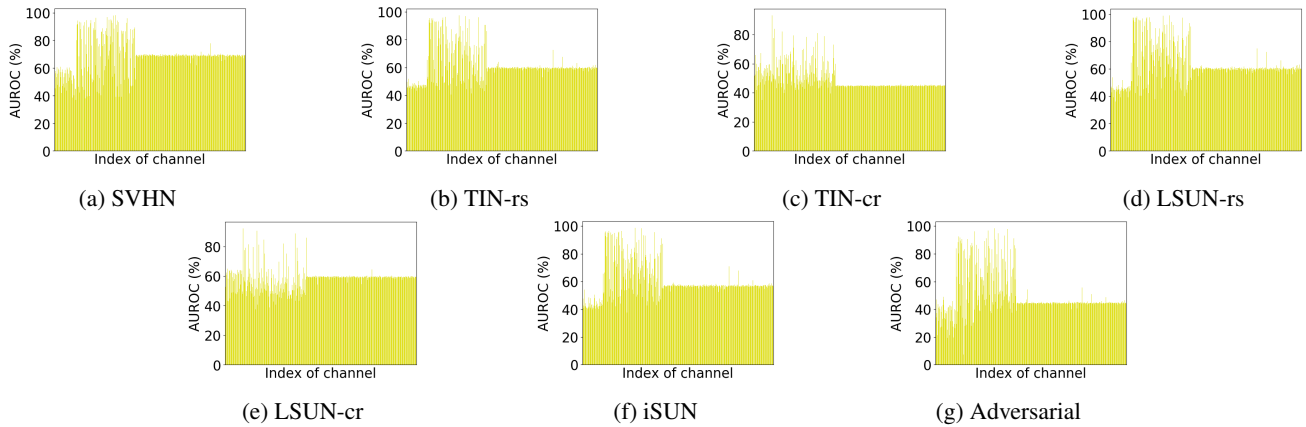


Figure 3: Trends of channel-wise OOD detection performance evaluated with AUROC for different OOD datasets when the InD dataset is CIFAR-100. The plots show that the AUROC trend of adversarial images is similar to most of the OOD datasets, indicating that the logistic regression classifier trained using adversarial images can generalize to most of the OOD datasets.

D. AUROC trends for CIFAR-100 datasets

In the main paper, we demonstrate that the similarities between channel-wise AUROC trends of adversarial examples and the OOD datasets play a significant role on OOD detection accuracy for CIFAR-10 dataset. We conduct the same analysis for the CIFAR-100 dataset to demonstrate that this observation holds for various datasets. We plot the trends for the OOD datasets and the adversarial examples for the network trained on CIFAR-100 dataset in Fig. 3. SVHN, TIN-rs, LSUN-rs, and iSUN have very similar trends with the adversarial images which explains the better performance on these OOD datasets.

E. Comparison between channel-wise KDE vs layer-wise KDE

In this section, we present further comparison between channel-wise KDE (the proposed method) and the layer-wise KDE, in addition to the results presented in Sec. 3.4. in the main paper. The results on CIFAR-100 and CIFAR-10 datasets are presented in Tables 11 and 12.

OOD	FPR at 95% TPR \downarrow	AUROC \uparrow	Detection Error \downarrow
Layer-wise KDE / Proposed (Channel-wise KDE)			
SVHN	24.09 / 4.87	94.66 / 98.05	14.54 / 4.93
TIN-rs	34.08 / 6.18	93.89 / 98.18	19.54 / 5.58
TIN-cr	93.99 / 78.15	46.87 / 75.01	49.49 / 41.57
LSUN-rs	28.47 / 1.70	94.55 / 99.41	16.73 / 3.35
LSUN-cr	84.90 / 65.22	66.50 / 81.54	44.95 / 35.11
iSUN	33.49 / 4.41	93.90 / 98.91	19.24 / 4.70

Table 11: Comparison between channel-wise vs layer-wise KDE on CIFAR-100 dataset.

OOD	FPR at 95% TPR \downarrow	AUROC \uparrow	Detection Error \downarrow
Layer-wise KDE / Proposed (Channel-wise KDE)			
SVHN	2.44 / 6.80	99.36 / 97.87	3.72 / 5.90
TIN-rs	5.11 / 1.91	98.99 / 99.05	5.05 / 3.45
TIN-cr	25.74 / 72.01	91.69 / 78.88	15.37 / 38.50
LSUN-rs	2.54 / 1.12	99.44 / 99.62	3.77 / 3.06
LSUN-cr	13.48 / 79.79	96.99 / 71.63	9.24 / 42.39
iSUN	3.83 / 2.06	99.26 / 98.93	4.41 / 3.53

Table 12: Comparison between channel-wise vs layer-wise KDE on CIFAR-10 dataset.

F. Details of the adversarial perturbation method - FGSM

As we discussed in Sec. 2.2. of the main paper, we produce pseudo-OOD samples using an adversarial attack method called Fast Gradient Sign Method (FGSM) [11]. In this section, we present some details of FGSM for the sake of completeness.

The FGSM method uses gradients of the neural network when creating an adversarial example. To this end, it computes the gradient of the loss function with respect to the input image and adds the gradient to the original input image to obtain the adversarial image. Perturbing the input image with the gradient leads to maximizing the loss function. The FGSM method for an input image x , its label y , and the loss function $L(x, y)$ is formalized as follows:

$$x_{adv} = x + \epsilon \times \text{sign}(\nabla(L(x, y)))$$

where ϵ is a parameter to control the strength of the perturbation and we set $\epsilon = 0.1$ in all experiments. We present some example images from CIFAR-10 dataset along with their adversarial version in Fig. 4.

G. Discussion on generative models-based OOD detection methods

In addition to the OOD detection methods we discussed in the main paper that operate on discriminative neural networks, there is also a line of work that focuses on the OOD detection on generative models. OOD detection accuracy of these methods are not yet on the level of the OOD detection methods designed for discriminative networks. The generative models suffer from diminished OOD detection accuracy since these models assign higher probabilities to the OOD samples than the InD samples [25]. For the sake of the completeness, we compare our results with a recent generative model-based OOD detection method proposed by Hendryks et al. [15] in Tables 13 and 14. For comparison, we collected the results from the experiments that are common in our main paper and Hendryks et al. [15]. In these experiments, Hendryks et al. [15] use PixelCNN++ as generative model on both CIFAR-10 and CIFAR-100 datasets. The results demonstrate that our method significantly outperforms Hendryks et al. [15] on these experiments.



Figure 4: Applying FGSM to some example images from CIFAR-10 dataset. Note that each row corresponds to a different image. Columns from left to right indicate original image, gradient of the loss w.r.t. input image, and adversarial image, respectively.

OOD	FPR at 95% TPR ↓	AUROC ↑
	Hendryks et al. [15] / Proposed	
SVHN	86.9 / 6.8	75.8 / 97.8
LSUN	43.2 / 1.1	90.9 / 99.6

Table 13: Comparison of the proposed method with a generative model-based OOD detection method on CIFAR-10 dataset.

OOD	FPR at 95% TPR ↓	AUROC ↑
	Hendryks et al. [15] / Proposed	
SVHN	42.9 / 4.8	86.9 / 98.0
LSUN	57.5 / 1.7	83.4 / 99.4

Table 14: Comparison of the proposed method with a generative model-based OOD detection method on CIFAR-100 dataset.